

# A HYPERELASTIC REGULARIZATION ENERGY FOR IMAGE REGISTRATION

MARTIN BURGER AND JAN MODERSITZKI AND LARS RUTHOTTO

**Abstract.** Image registration is one of the most challenging problems in image processing, where ill-posedness arises due to noisy data as well as non-uniqueness and hence the choice of regularization is crucial. This paper presents hyperelasticity as a regularizer and introduces a new and stable numerical implementation. On one hand, hyperelastic registration is an appropriate model for large and highly nonlinear deformations, for which a linear elastic model needs to fail. On the other hand, the hyperelastic regularizer yields very regular and diffeomorphic transformations. While hyperelasticity might be considered as just an additional outstanding regularization option for some applications, it becomes inevitable for applications involving higher order distance measures like mass-preserving registration.

The paper gives a short introduction to image registration and hyperelasticity. The hyperelastic image registration problem is phrased in a variational setting and an existence proof is provided. The focus of the paper, however, is on a robust numerical scheme. A key challenge is an unbiased discretization of hyperelasticity, which enables the numerical monitoring of variations of length, surface and volume of infinitesimal reference elements. We resolve this issue by using a nodal based discretization with a special tetrahedral partitioning.

The potential of the hyperelastic registration is demonstrated in a direct comparison with a linear elastic registration on an academical example. The paper also presents a real life application from 3D Positron Emission Tomography (PET) of the human heart which requires mass-preservation and thus hyperelastic registration is the only option.

**Key words.** image registration, regularization, hyperelasticity

**AMS subject classifications.** 92C55, 65M55, 15A23, 65K10

**1. Introduction.** The goal of image registration is to automatically establish geometrical correspondences between two or more given data sets. Image registration is an important tool for various areas of applications such as anatomy, astronomy, biomedical imaging, forensics, robotics, or remote sensing, to name a few. In particular in medical imaging, image registration is inevitable whenever images taken at different times, from different devices, with different modalities, or even from different individuals need to be compared or fused; see, e.g. [35, 19, 42, 41, 17, 28, 50, 36, 20, 37] and references therein.

Although the registration problem is easily stated it is hard to be solved. A key difficulty is the ill-posedness of the problem [27, 48, 32, 11, 23]. For a particular point, scalar intensities are given but a transformation vector is to be computed. A common approach is to phrase image registration as an optimization problem involving a distance measure reflecting *similarity* of images and a regularization term reflecting *reasonability* of the transformation. An example is the so-called elastic registration scheme introduced by Broit [4, 1]. In his groundbreaking dissertation, the elastic potential based on a linear elasticity model is introduced and has served as a model in a huge number of publications and as a synonym for nonlinear registration.

Despite its enormous success, elastic registration has some limitations. As the scheme is based on linear elasticity, difficulties are to be expected and have been reported for largely deformed data sets. Therefore, Christensen [6] developed a so-called fluid registration scheme and Thirion [46] the so-called demons registration to handle large deformation. Although success has been reported for various applications, both techniques are not based on an optimization approach and use some non-physical heuristics such as regriding or choices of demons forces and smoothing. Another limitation related to linear elasticity is that elastic registration does not

necessarily compute a diffeomorphic transformation. A proper parameter choice can resolve this problem, but may also result in an almost rigid transformation. Finally, as the elastic regularization is only of first order, the classical theory of variational calculus does not guarantee existence of solutions for various distance measure like normalized gradient fields (NGF) [12, 25] and mass preservation (MP) [44] or the integration of constraints like landmark correspondences [15, 21, 39]. Second order curvature registration has been introduced to provide appropriate regularization [15] but its physical motivation is difficult and the curvature scheme does not guarantee diffeomorphic transformations.

In this paper we discuss hyperelastic regularization in the context of image registration and introduce a new numerically stable implementation. The goal is to model large nonlinear deformations with physically meaningful transformations being at least diffeomorphic, i.e. smooth and one-to-one. In contrast to [49], we use a hyperelastic registration approach where the determinant of the Jacobian is explicitly monitored and the regularization energy approaches infinity for non-diffeomorphic transformations. The price to be paid is a nontrivial discretization and the regularization energy to be non-convex with respect to the Jacobian of the transformation. However, the energy functional can be designed to be *polyconvex*; see [13, 9]. Polyconvexity is a crucial ingredient to Ball’s theorem [2], which essentially establishes existence for non-linear elasticity. Following [11, 26], we present an existence result and generalize it to distance measures that may depend on the Jacobian of the transformation. We remark that our theory does not include the case of a non-convex double well potential for surface regularization for which we obtained the best numerical results, see discussion in Section 2 and 3.

The focus of this paper is on a stable numerical implementation of the hyperelastic regularization. It is well-understood, that discrete analogues of continuous operators may not share all of their properties. A trivial example is a finite difference approximation of a derivative using long stencils. The discrete operator annihilates highly oscillatory functions whereas the continuous operator does not [23]. Moreover, a function being positive on a discrete set needs not to be positive everywhere. Thus, even if a continuous formulation of a problem guarantees properties like  $\det \nabla y > 0$ , a related discrete version may not. In this paper we use a geometric, voxel based discretization approach, which is well-suited to the underlying discretization of the medical data of our numerical evaluation of the scheme. We measure the main ingredients of hyperelastic regularization, i.e. the invariants such as length, surface, volume, on the smallest unit, which is a tetrahedron and prove that this discretization is sufficient. In our implementation all these measures are controlled during an optimization process. Finally, we highlight the potential of our registration approach on a 2D academic example and a clinically relevant registration problem of 3D cardiac positron emission tomography (PET).

**2. Mathematical Model of Hyperelastic Image Registration.** We briefly introduce the hyperelastic image registration problem, see e.g. [36, 37] for more details on a general approach. Given are two images  $\mathcal{T}, \mathcal{R} : \Omega \subset \mathbb{R}^d \rightarrow \mathbb{R}$ , compactly supported on  $\Omega$ , where for medical applications typically  $d = 3$ . The goal is to find a transformation  $y : \Omega \rightarrow \mathbb{R}^d$  or a deformation, such that ideally  $\mathcal{T}(y(x)) \approx \mathcal{R}(x)$  for all  $x \in \Omega$ . This goal is achieved by minimizing a so-called distance measure  $\mathcal{D}$ . As this problem is ill-posed [16] an appropriate regularization  $\mathcal{S}$  is inevitable.

A variational formulation of the image registration problem is to find a mini-

mizer  $y$  of

$$\mathcal{J}(y) = \mathcal{D}(\mathcal{T}, \mathcal{R}; y) + \mathcal{S}(y) \quad \text{for } y \in \mathcal{A}, \quad (2.1)$$

where  $\mathcal{A}$  denotes the set of admissible transformations. The remainder of this section specifies and discusses options for the ingredients  $\mathcal{D}$ ,  $\mathcal{S}$ , and  $\mathcal{A}$ . Since concrete parameter choices are not essential for the theoretical analysis, particular choices are postponed to Section 5. Moreover, we restrict the presentation to  $d = 3$  and as the domain  $\Omega$  is fixed in our setting, we set  $\Omega = (0, 1)^3$  and skip the dependence on  $\Omega$  in the following formulae.

Typical choices for the distance  $\mathcal{D}$  include squares of  $L_p$ -norms, e.g.

$$\mathcal{D}^{\text{SSD}}(\mathcal{T}, \mathcal{R}; y) := \int (T(y(x)) - R(x))^2 dx, \quad (2.2)$$

mutual information [8, 47], normalized gradient fields [12, 25], or mass-preserving measures such as

$$\mathcal{D}^{\text{MP}}(\mathcal{T}, \mathcal{R}; y) := \int (T(y(x)) \det \nabla y(x) - R(x))^2 dx, \quad (2.3)$$

which (under suitable assumptions on  $\mathcal{T}$  and  $y$ ) ensure mass-preservation as it is essential for accurate registration of human cardiac PET from different heart phases, see [44] and Section 5 for an application. As the data fitting term is of minor interest in this paper and we aim for a simplicity of presentation, we focus on (2.3), but emphasize that our existence theory covers a wide range of relevant distance functionals including those that depend linearly on  $\nabla y$ , see Section 3 for details.

Regularization is in general based on  $\nabla y = (\partial_j y_i)_{i,j=1}^d$  and a strain tensor. This tensor is typically defined via the displacement  $u$ , with  $y(x) = x + u(x)$  and thus  $\nabla y = I_d + \nabla u$ ; see, e.g., [7]. Examples are the *Cauchy strain tensor*  $V$  (for  $\|\nabla u\| \ll 1$ ) or the *Green-St.-Venant strain tensor*  $E$  with

$$V = V(y) = (\nabla u + \nabla u^\top)/2 \quad \text{and} \quad E = E(y) = (\nabla u + \nabla u^\top + \nabla u^\top \nabla u)/2. \quad (2.4)$$

Important choices for a regularizer  $\mathcal{S}$  include

$$\begin{aligned} \mathcal{S}^{\text{elas}}(y) &= \int \nu(\text{trace}V)^2 + \mu \text{trace}(V^2) dx, \\ \mathcal{S}^{\text{curv}}(y) &= \sum_{i=1}^d \int (\Delta y_i)^2 dx \\ \mathcal{S}^{\text{quad}}(y) &= \int \nu(\text{trace}E)^2 + \mu \text{trace}(E^2) dx, \end{aligned}$$

with  $\nu$  and  $\mu$  the Lamé constants [15, 36, 7, 49].

The first regularizer is based on linear elasticity and leads to the well-known elastic registration [4, 7]. It employs first order derivatives and the existence of optimal solutions can be shown for  $L_2$  norm distance functionals using Korn's inequality, cf. [33]. However, to our best knowledge there is no existence proof for problems involving distance measure like (2.3) or landmark based constraints [34, 14]. The second regularizer is the curvature regularizer, which has been introduced to satisfy landmark

constraints [15]. It has an infinite dimensional nullspace or challenging boundary conditions that have been addressed in [30]. The last regularizer is a hyperelastic model and quadratic in  $\nabla y$ ; see [49] for details. A common drawback of the above models is that transformations with  $\det \nabla y = 0$  yield finite energy.

In this paper, we consider energy functionals that reflect two desired properties for large deformations (i.e. large strain with  $\|\nabla u\| \gg 0$ ). We aim for energies that tend to infinity for non-diffeomorphic transformations:

$$\begin{aligned} \mathcal{S}(y) &\longrightarrow \infty \quad \text{for } \det \nabla y \rightarrow 0, \\ \mathcal{S}(y) &\geq c_1 \{ \|\nabla y\|^p + \|\text{cof } \nabla y\|^q + (\det \nabla y)^r \} + c_2, \end{aligned} \quad (2.5)$$

with  $c_1 > 0$ ,  $c_2 \in \mathbb{R}$  and numbers  $p, q, r > 1$ , see, e.g., [7, §4, p138]. These conditions guarantee sufficient growth of the penalty for small and large deformations, respectively. In this paper, we suggest

$$\mathcal{S}^{\text{hyper}}(y) := \int \alpha_1 \text{length}(y) + \alpha_2 \text{surface}(y) + \alpha_3 \text{volume}(y) \, dx, \quad (2.6)$$

where  $\alpha_i > 0$  are some parameters and the length, surface, and volume are related to the three invariants gradient, cofactor, and determinant of the transformation. Before discussing our particular setting, we present precise formulae:

$$\begin{aligned} \text{length}(y) &= \phi_\ell(\nabla y), & \phi_\ell(X) &= \|X - I_d\|_{\text{Fro}}^2, \\ \text{surface}(y) &= \phi_{w,c}(\text{cof } \nabla y), & \phi_w(X) &= (\|X\|_{\text{Fro}}^2 - 3)^2, \\ & & \phi_c(X) &= \max\{\|X\|_{\text{Fro}}^2 - 3, 0\}^2 \\ \text{volume}(y) &= \phi_v(\det \nabla y), & \phi_v(x) &= ((x - 1)^2/x)^2, \end{aligned} \quad (2.7)$$

with the Frobenius-norm  $\|X\|_{\text{Fro}} := \sqrt{\sum X_{i,j}^2}$ , and cofactor and determinant as

$$\begin{aligned} \text{cof } \nabla y &= \begin{pmatrix} \partial_2 y_2 \partial_3 y_3 - \partial_3 y_2 \partial_2 y_3 & \partial_3 y_2 \partial_1 y_3 - \partial_1 y_2 \partial_3 y_3 & \partial_1 y_2 \partial_2 y_3 - \partial_2 y_2 \partial_1 y_3 \\ \partial_3 y_1 \partial_2 y_3 - \partial_2 y_1 \partial_3 y_3 & \partial_1 y_1 \partial_3 y_3 - \partial_3 y_1 \partial_1 y_3 & \partial_2 y_1 \partial_1 y_3 - \partial_1 y_1 \partial_2 y_3 \\ \partial_2 y_1 \partial_3 y_2 - \partial_3 y_1 \partial_2 y_2 & \partial_3 y_1 \partial_1 y_2 - \partial_1 y_1 \partial_3 y_2 & \partial_1 y_1 \partial_2 y_2 - \partial_2 y_1 \partial_1 y_2 \end{pmatrix}, \\ \det \nabla y &= \partial_1 y_1 \partial_2 y_2 \partial_3 y_3 + \partial_2 y_1 \partial_3 y_2 \partial_1 y_3 + \partial_3 y_1 \partial_1 y_2 \partial_2 y_3 \\ &\quad - \partial_1 y_3 \partial_2 y_2 \partial_3 y_1 - \partial_2 y_3 \partial_3 y_2 \partial_1 y_1 - \partial_3 y_3 \partial_1 y_2 \partial_2 y_1. \end{aligned}$$

The length term based on  $\nabla y$  yields a control of length (and angle) variations, here a quadratic penalty  $\phi_\ell$  for departure from the identity is chosen. The cofactor matrix quantifies surface changes. Each column consists of a normal vector of length  $\ell$  to a reference surface, where  $\ell$  corresponds to the area of the transformed surface. In our application we would like to penalize changes in area. Hence the penalty should be zero if  $\ell = 1$  and positive otherwise. This can be achieved by using the double well function  $\phi_w$ . However, the double well is not convex and standard arguments do not apply. For the theoretical part, we thus introduce the convex envelope  $\phi_c$  of  $\phi_w$ . Note that the convex  $\phi_c$  does not penalize surface shrinkage while the double well does and is therefore practically superior. Volume changes are controlled by the determinant. For Ogden materials, the penalty  $\phi_{\text{Ogden}}(x) = x^2 - \log x$  is chosen, which yields

$$S^{\text{Ogden}}(y) = S^{\text{quad}}(y) + \mathcal{O}(\|\nabla y\|^3),$$

and justifies  $S^{\text{quad}}$  for transformations with  $\|\nabla u\| \ll 1$ ; see, e.g. [11, 7]. Our regularizer controls all invariants but uses a volume penalty with  $\phi_v(1/x) = \phi_v(x)$ , such

that shrinkage and growth have the same price. Note that both,  $\phi_{\text{Ogden}}$  and  $\phi_v$  satisfy  $\lim_{x \rightarrow 0} \phi(x) = \infty$  as desired, cf. (2.5).

The price to be paid for using this class of regularizers has already been pointed out by Ciarlet [7, §4, p138f] – with his notation  $F = \nabla u$ : “*The lack of convexity of the stored energy function with respect to the variable  $F$  is the root of a major difficulty in the mathematical analysis of the associated minimization problem.*” Before presenting our numerical implementation in Section 4, we therefore prove existence of a minimizing element for our registration energy; see Section 3.

Based on the above discussion, it is natural to seek for transformations in the Sobolev space  $W^{1,2}(\Omega, \mathbb{R}^3)$  where the cofactor and the determinant are sufficiently integrable and the determinant is essentially positive. We therefore start with

$$\mathcal{A}_0 := \{y \in W^{1,2}(\Omega, \mathbb{R}^3) : \text{cof } \nabla y \in L_4(\Omega, \mathbb{R}^{3 \times 3}), \det \nabla y \in L_2(\Omega, \mathbb{R}), \det \nabla y > 0 \text{ a.e.}\}.$$

In Ball’s formulation of non-linear elasticity, boundary conditions are imposed in order to control the norm of the transformation and to obtain existence [2, 7, 9]. However, the boundedness of feasible transformations is less critical in our application. Reasonable displacements are bounded by  $\text{diam}(\Omega)$  as for larger deformations there is no overlap between the template and the reference image; see also discussion in [43]. Further, the domain  $\Omega$  itself can be bounded by a constant  $M \in \mathbb{R}$ . The straight forward approach to consider  $\|y\|_\infty \leq M + \text{diam}(\Omega)$  would complicate the analysis as  $L_\infty(\Omega, \mathbb{R}^3)$  is a not reflexive space. Therefore we use the following average version and in the next section we obtain existence of solutions in

$$\mathcal{A} := \{y \in \mathcal{A}_0 : \left| \int y(x) dx \right| \leq |\Omega|(M + \text{diam}(\Omega))\}. \quad (2.8)$$

**3. Existence Result.** The goal of this section is to provide insight to the existence theory of solutions  $y$  of problem (2.1) using standard arguments from the theory of nonlinear elasticity. We prove that the presented regularization energy  $\mathcal{S}^{\text{hyper}}$  guarantees the existence of diffeomorphic solutions  $y$  of problem (2.1) for practically relevant distance measures  $\mathcal{D}$ . Especially for the *mass-preserving* registration (2.3) complications in the existence proof are related to the dependency of  $\mathcal{D}^{\text{MP}}$  on  $\det \nabla y$ , the measurability of  $\det \nabla y$  (see also [43]), and the constraint  $\det \nabla y > 0$  a.e.. Particularly in the large deformation setting, these requirements yield strong demands on the regularization, as discussed in the previous section. To our best knowledge, existence has only been shown in special settings [44, 43].

The key observation is that  $\mathcal{D}^{\text{MP}}$  in (2.3) and  $\mathcal{S}^{\text{hyper}}$  depend in a non-convex way on  $\nabla y$ , but the dependence on  $\text{cof } \nabla y$  and  $\det \nabla y$  is convex. Therefore,  $\mathcal{D}^{\text{MP}}$  as well as all the above mentioned distance measures and  $\mathcal{S}^{\text{hyper}}$  are *polyconvex* functionals, see (A1) below and [13, 9]. The existence of minimizing elements for such polyconvex functionals is the topic of the following theorem. Our arguments require all parts to be convex as it is obvious for the length and the volume penalties. For the surface part we use the convex envelope  $\phi_c$  of the practically more interesting double well  $\phi_w$ ; see discussion in the previous section and (2.7).

**THEOREM 1.** *Given are images  $\mathcal{R}, \mathcal{T} \in C(\mathbb{R}^3, \mathbb{R})$ , compactly supported in  $\Omega$ , a polyconvex distance measure  $\mathcal{D} = \mathcal{D}(y) = \mathcal{D}(\mathcal{T}, \mathcal{R}; y, \nabla y, \det \nabla y)$  with  $\mathcal{D} \geq 0$ ,  $\mathcal{S}^{\text{hyper}}$  as in (2.6) with convex penalties  $\phi_\ell$ ,  $\phi_c$ , and  $\phi_v$ , and  $\mathcal{A}$  as in (2.8). We assume that the registration functional  $\mathcal{J}$  (2.1) satisfies  $\mathcal{J}(\text{Id}) < \infty$  for  $\text{Id}(x) := x$  on  $\Omega$ . Then there exists at least one minimizer  $y^* \in \mathcal{A}$  of the functional  $\mathcal{J}$ .*

In order to show the existence of a minimizer  $y \in \mathcal{A}$  of  $\mathcal{J}$ , we recall Ball's existence theorem for nonlinear elasticity [2, 7, 9]. Using a function  $y_{\text{BC}}$  to describe boundary conditions, Ball proved existence of minimizing elements for functionals of type

$$I(y) = \int g(x, y, \nabla y) dx \quad (3.1)$$

under assumptions

- A1: the stored energy function  $g$  is *polyconvex*, i.e. there exists a function  $\tilde{g} : \Omega \times \mathbb{R}^3 \times \mathbb{R}^{3 \times 3} \times \mathbb{R}^{3 \times 3} \times ]0, +\infty[$  such that  $g(x, y, A) = \tilde{g}(x, y, A, \text{cof}(A), \det A)$  and  $\tilde{g}(x, y, \cdot, \cdot, \cdot)$  is convex for every  $y \in \mathbb{R}^3$  and almost every fixed  $x \in \Omega$ ,
- A2: the integrand  $\tilde{g}$  is Carathéodory, i.e.
- (i)  $\tilde{g}(x, \cdot, \cdot, \cdot, \cdot)$  is continuous for almost every  $x \in \Omega$ ,
  - (ii)  $\tilde{g}(\cdot, z, D, C, v)$  is measurable in  $x$  for every  $(z, D, C, v) \in \mathbb{R}^3 \times \mathbb{R}^{3 \times 3} \times \mathbb{R}^{3 \times 3} \times ]0, +\infty[$ .
- A3: the functional satisfies a coercivity condition (see (2.5)), i.e. there exist constants  $K \in \mathbb{R}$  and  $C > 0$  and exponents  $p \geq 2$ ,  $q \geq \frac{p}{p-1}$ ,  $r > 1$ , such that

$$I(y) \geq C (\|\nabla y\|_{L^p}^p + \|\text{cof } \nabla y\|_{L^q}^q + \|\det \nabla y\|_{L^r}^r) + K. \quad (3.2)$$

- A4: For almost all  $x \in \Omega$ ,  $\tilde{g}(x, y, \nabla y, \text{cof}(\nabla y), \det \nabla y) \rightarrow \infty$  as  $\det \nabla y \rightarrow 0$ . The convergence is uniform with respect to  $y$  in any bounded subset of  $\mathbb{R}^3$ .

As mentioned above, we have no explicit boundary conditions in our application, which requires minor changes of the standard proof given in [2, Thm 7.3]. Assumption (A4) is essential to obtain the strict positivity of the Jacobian determinant of minimizers of  $\mathcal{J}$ , which was directly shown in [11].

**THEOREM 2.** *Assume that the functional  $I$  in (3.1) satisfies (A1)–(A4) and that there exists  $\bar{y} \in \mathcal{A}$  as in (2.8) with  $I(\bar{y}) < \infty$ . Then there exists at least one minimizer  $y^* \in \mathcal{A}$  of  $I$ .*

*Proof.* Existence is obtained from lower semicontinuity and coercivity of the functional  $I$  in  $\mathcal{A}$ . Noticing that

$$y \mapsto \left( \frac{1}{|\Omega|} \left| \int y(x) dx \right| \right)^2$$

is a continuous and convex function from  $L_2(\Omega, \mathbb{R}^3)$  to  $\mathbb{R}^+$  and thus weakly lower semicontinuous, one obtains that  $\mathcal{A}$  is weakly closed in  $L_2(\Omega, \mathbb{R}^3)$ . Thus, the lower semicontinuity can be shown as in the proof of [2, Thm 7.3]. In order to obtain coercivity in  $W^{1,2}(\Omega, \mathbb{R}^3)$  for arbitrary  $y \in \mathcal{A}$  we employ Poincaré's inequality [13, p. 275], the triangle inequality and the fact that the mean of a transformation  $y \in \mathcal{A}$ , denoted by  $\bar{y} := \frac{1}{|\Omega|} \int y(x) dx$ , is bounded

$$\begin{aligned} \|\nabla y\|_{L_2}^2 &\geq C \|y - \bar{y}\|_{L_2}^2 = C \|y\|_{L_2}^2 - C |\Omega| \left( \frac{1}{|\Omega|} \left| \int y(x) dx \right| \right)^2 \\ &\geq C \|y\|_{L_2}^2 - C |\Omega| (M + \text{diam}(\Omega))^2. \end{aligned}$$

Hence (3.2) also implies a bound on  $\|y\|_{W^{1,2}}$ . Note that the exponents  $p = 2$ ,  $q = 4$ ,  $r = 2$  satisfy the conditions in (A3). All further steps are exactly as in the proof of [2, Thm 7.3].  $\square$

Based on Theorem 2, we are ready to prove our Theorem 1.

*Proof. (Theorem 1)* We verify that  $\mathcal{J}$  satisfies assumptions (A1)–(A4). Since  $\mathcal{D}$  is polyconvex by assumption and  $\mathcal{S} := \mathcal{S}^{\text{hyper}}$  is polyconvex by design of  $\phi_\ell$ ,  $\phi_c$ , and  $\phi_v$ , also  $\mathcal{J} = \mathcal{D} + \mathcal{S}$  is polyconvex. Hence there exists a function  $\tilde{g} : \Omega \times \mathbb{R}^3 \times \mathbb{R}^{3 \times 3} \times \mathbb{R}^{3 \times 3} \times ]0, +\infty[ \rightarrow \mathbb{R}$  that is convex in the last three arguments and satisfies  $\mathcal{J}(y) = \int \tilde{g}(x, y, \nabla y, \text{cof } \nabla y, \det \nabla y) dx$ .

We note that  $\tilde{g}(x, \cdot, \cdot, \cdot, \cdot)$  is continuous for almost every  $x \in \Omega$ . Further, for every fixed  $(z, D, C, v) \in \mathbb{R}^3 \times \mathbb{R}^{3 \times 3} \times \mathbb{R}^{3 \times 3} \times ]0, +\infty[$  we see that  $\tilde{g}(\cdot, z, D, C, v)$  is measurable in  $x$  and hence  $\tilde{g}$  is Carathéodory.

Since  $\mathcal{D} \geq 0$  and the regularization functional  $\mathcal{S}$  satisfies (2.7), there exist constants  $C_k > 0$  and  $K_k \in \mathbb{R}$ , where  $k \in \mathbb{N}$ , such that

$$\begin{aligned} \mathcal{J}(y) &\geq \int \|\nabla y - I_d\|_{\text{Fro}}^2 + \phi_c(\text{cof } \nabla y) + \phi_v(\det \nabla y) dx \\ &\geq C_1 \int \|\nabla y - I_d\|_{\text{Fro}}^2 + \|\text{cof } \nabla y\|_{\text{Fro}}^4 + (\det \nabla y)^2 dx + K_1. \end{aligned}$$

Using the fact that  $(a - b)^2 \geq \frac{1}{2}a^2 - b^2$  holds for  $a, b \in \mathbb{R}$  we obtain assumption (A3)

$$\begin{aligned} &\geq C_1 \int \frac{1}{2} \|\nabla y\|_{\text{Fro}}^2 - \|I_d\|_{\text{Fro}}^2 + \|\text{cof } \nabla y\|_{\text{Fro}}^4 + (\det \nabla y)^2 dx + K_1 \\ &\geq C_2 (\|\nabla y\|_{L_2}^2 + \|\text{cof } \nabla y\|_{L_4}^4 + \|\det \nabla y\|_{L_2}^2) + K_2. \end{aligned}$$

We finally note that  $\tilde{g}$  fulfills (A4) by design of  $\phi_v$  and thus all assumptions of Theorem 2 are satisfied. Thus, there exists at least one minimizer  $y^* \in \mathcal{A}$ .  $\square$

**4. Numerical Implementation.** Our numerical implementation is based on a discretize-then-optimize strategy, following a multi-level registration strategy as outlined in [37]. The crucial part is a proper discretization, which is outlined in detail below. On a coarse level discretization, a numerical minimizer is computed, prolonged to a finer discretization, and then used as a starting guess on the finer level. We use a generalized Gauss-Newton scheme to compute a numerical minimizer. Moreover, we use a backtracked Armijo line search guaranteeing sufficient descent and  $\det \nabla y > 0$ ; see [38] for details.

We now describe our discretization, the discrete objective function, its analytic gradient, and our approximation to the Hessian. We control the change of volume under a discrete transformation  $y$  on the smallest measurable unit namely a voxel. As it is well-known [24], the control of volume change of a voxel is not straightforward. To ensure a diffeomorphic transformation, we use a partitioning approach similar to the one in [24]. The volume of a set  $V$  transformed by  $y$  is given by

$$\text{vol}(y(V)) = \int_{y(V)} dx = \int_V \det \nabla y dx.$$

Note, however, that the latter equality assumes sufficient regularity of  $y$ , which is critical in this setting. Our discretization is therefore based directly on  $\int_{y(V)} dx$  and measures the volume spanned by the transformed vertices.

Our primary discretization is based on a nodal grid of the computational domain, where for ease of presentation we set  $\tilde{\Omega} = [0, 1]^3$  and an equal number  $m$  of grid points for every dimension; see [37] for details on more general discretizations. Using multi-indices  $i = (i_1, i_2, i_3)$ , the so-called nodal grid points are given by

$$y_i = hi, \quad h = 1/m, \quad i_j = 0, \dots, m, \quad j = 1, 2, 3.$$

We denote the number of grid points by  $N := (m + 1)^3$ . The cube spanned by eight nodes  $y_{i+k}$ ,  $k \in \{0, 1\}^3$  is called a voxel  $V^i$ ; see Fig. 4.1. This voxel is partitioned into tetrahedra  $T_j^i$  and our discrete model for the transformation is a continuous vector field, which is linear on each  $T_j^i$ .

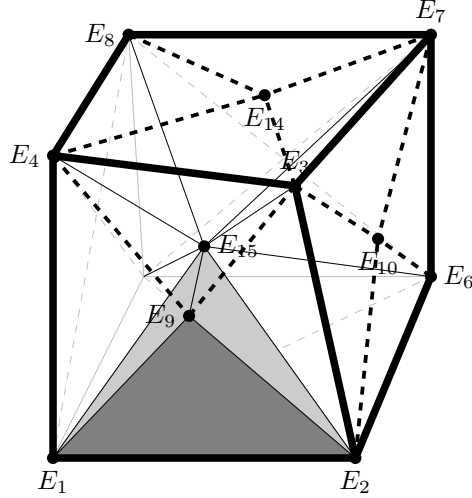


FIG. 4.1. Partitioning of a deformed voxel from a nodal grid  $E_1, \dots, E_8$  with face average points  $E_9, \dots, E_{14}$  and center  $E_{15}$

**THEOREM 3.** *Let  $V$  be a voxel and  $\{T_j, j \in J\}$  be a tetrahedral partition of  $V$  with  $\text{vol}(T_j) > 0$  for all  $j \in J$ . Moreover let  $y : \bar{\Omega} \rightarrow \mathbb{R}^3$  be a vector field such that  $y|_{T_j}$  is linear. It holds*

$$\det \nabla y|_V > 0 \quad \text{a.e.} \quad \iff \quad \forall j \in J : \quad \text{vol}(y(T_j)) > 0. \quad (4.1)$$

*Proof.* Since  $\{T_j, j \in J\}$  is a partition of  $V$ , it holds  $\det \nabla y|_V > 0$  a.e.  $\iff \forall j \in J : \det \nabla y|_{T_j} > 0$ . Moreover,  $y|_{T_j}$  is linear and thus  $\det \nabla y|_{T_j} = c_j$  is a constant. The volume of a deformed tetrahedron is

$$\text{vol}(y(T_j)) = \int_{y(T_j)} dx = \int_{T_j} c_j dx = c_j \text{vol}(T_j),$$

covering the cases  $c_j > 0$ ,  $c_j = 0$ , and  $c_j < 0$ . Thus,  $\det \nabla y|_{T_j} > 0 \iff \text{vol}(y(T_j)) > 0$  which together with  $\{T_j, j \in J\}$  being a partitioning yields the assertion.  $\square$

Theorem 3 ensures regularity of various partitions including the ones used in [24] (six tetrahedra), [22] (five tetrahedra), and a new tetrahedral model (24 tetrahedra) as suggested by Heldmann [29]. The latter one is used in this paper.

We illustrate Heldmann's [29] tetrahedral model for an arbitrary but specific voxel  $V^i$  and in the following skip the dependence on  $i$  for ease of presentation; see Fig. 4.1. The nodal points or vertices are denoted by  $E_1, \dots, E_8$ . Heldmann's suggestion is to introduce seven auxiliary points. The first six are face average points and the fifteenth is the center of  $V$ . For example,  $E_9 := (E_1 + E_2 + E_3 + E_4)/4$ ,  $E_{14} := (E_3 + E_4 + E_7 + E_8)/4$ , and  $E_{15} := \sum_{k=1}^8 E_k/8$ . Using these additional

points, we get a symmetric representation of each of the six faces of the voxel into a total of 24 triangles; for example,  $F_{(1,2,9)} := \Delta(E_1, E_2, E_9)$ ,  $F_{(2,3,9)} := \Delta(E_2, E_3, E_9)$ ,  $F_{(3,4,9)} := \Delta(E_3, E_4, E_9)$ , and  $F_{(4,2,9)} := \Delta(E_4, E_2, E_9)$  are the faces of the four triangles spanning the front face of the voxel shown in Fig. 4.1. The tetrahedron  $T_{(1,2,9)}$  is then obtained by connecting triangle  $F_{(1,2,9)}$  with the voxel's center  $E_{15}$ .

The advantage of this partition, which is much finer than the ones used in the constrained optimization approaches [22] and [24], lies in its symmetry. Thereby a bias related to particular discretization as it has been observed when using only five or six tetrahedra [3] is avoided. Another advantage is its smoothness. Though the transformation model is only piecewise linear, additional smoothness is introduced via the coupling through the face center points. A disadvantage is its computational costs.

Based on this discretization of  $y$ , we outline the discretization of  $\mathcal{J}$  (2.1). For the discretization of  $\mathcal{D}^{\text{MP}}$  we follow [37] and use our discretization of  $\det \nabla y$ . Note that  $\det \nabla y$  appears in  $\mathcal{D}^{\text{MP}}$  and  $\mathcal{S}$  and its computation can be reused. The regularizer is decomposed into three parts related to length, surface, and volume:

$$S^h(y) = h^3 S_\ell(y) + h^3 \sum_{i=1}^{m^3} \sum_{j=1}^{24} (S_{s,j}^i + S_{v,j}^i),$$

where the factor  $h^3$  results from integration. For the discretized length term we use

$$S_\ell(y) = \|\nabla^h y - \nabla^h \text{Id}\|^2 = \|\nabla^h u\|^2 = u^T (\nabla^h)^T \nabla^h u, \quad dS_\ell(y) = (\nabla^h)^T \nabla^h u,$$

as the length term is essentially a squared norm of the discrete, relative gradient, see [37] for details.

Our discretizations of the surface and volume terms are discussed exemplarily for the grayish tetrahedron  $T_{(1,2,9)}$  in Fig. 4.1. The computation for the other 23 tetrahedra is along the same lines. Note that only the 24 triangles belonging to the surface of the voxel are measured. To measure the area of the triangle  $F_{(1,2,9)}$ , we extract the positions of the vertices  $P_k$   $y := y(E_k)$ ,  $k \in \{1, 2, 9\}$ , compute a difference vector, and measure the area as a cross-product of these differences. Note that the reference area of a triangle of a face of a uniform voxel is  $h^2/4$ . Thus, with the vectors  $(d_i^j)_{i=1,2,3}$ , the variation of the surface is

$$\begin{aligned} S_{s,1}^i(y) &= S_{s,(1,2,9)}^i(y) = \phi_s(A(P_{(1,2,9)} y)), \\ P_{(1,2,9)} y &= [d^1, d^2] = [P_1 y - P_9 y, P_2 y - P_9 y], \\ A(P_{(1,2,9)} y) &= 4 \|d^1 \times d^2\|^2 / h^4, \end{aligned}$$

where the penalty  $\phi_s$  for the surface is either the double well or the convex model,

$$\phi_w(A) = (A - 1)^2 / 2, \quad \phi_c(A) = \max\{A - 1, 0\}^2 / 2.$$

The derivative is computed using the chain rule:

$$dS_{s,1}^i(y) = d\phi_s dA P_{(1,2,9)}, \quad d\phi_w = A - 1, \quad d\phi_c = \max\{A - 1, 0\}.$$

$$\begin{aligned} dA &= \frac{2}{h^2} (d_2^1 d_3^2 - d_3^1 d_2^2, d_3^1 d_1^2 - d_1^1 d_3^2, d_1^1 d_2^2 - d_2^1 d_1^2) \\ &\cdot \begin{pmatrix} 0 & d_3^2 & -d_2^2 & 0 & -d_3^1 & d_2^1 \\ -d_3^2 & 0 & d_1^2 & d_3^1 & 0 & -d_1^1 \\ d_2^2 & -d_1^2 & 0 & -d_2^1 & d_1^1 & 0 \end{pmatrix}. \end{aligned}$$

The computation of the variation of volume is along the same lines. A projector  $P_{(1,2,9,15)}$  extracts the vertices of the tetrahedron and its volume is computed using the rule of Sarrus:

$$\begin{aligned} S_{v,1}^i(y) &= S_{v,(1,2,9,15)}^i(y) = \phi_v(V(P_{(1,2,9,15)} y)), \\ P_{(1,2,9,15)} y &= [v^1, v^2, v^3] = [P_1 y - P_{15} y, P_2 y - P_{15} y, P_9 y - P_{15} y], \\ V(P_{(1,2,9,15)} y) &= 4 \det([v^1, v^2, v^3])/h^3, \\ \phi_v(v) &= (v-1)^4/v^2 \end{aligned}$$

with derivative

$$\begin{aligned} dS_{v,1}^i(y) &= d\phi_v dV P_{(1,2,9,15)}, \\ d\phi_v &= 2(v+1)((v-1)/v)^3, \\ dV &= \frac{1}{h^3} \begin{bmatrix} v_2^2 v_3^3 - v_3^2 v_2^3, & v_1^3 v_3^2 - v_3^3 v_1^2, & v_1^2 v_2^3 - v_2^2 v_1^3, \\ v_2^3 v_3^1 - v_3^3 v_2^1, & v_1^1 v_3^3 - v_3^1 v_1^3, & v_1^3 v_2^1 - v_2^3 v_1^1, \\ v_2^1 v_3^2 - v_3^1 v_2^2, & v_1^2 v_3^1 - v_3^2 v_1^1, & v_1^1 v_2^2 - v_2^1 v_1^2 \end{bmatrix}. \end{aligned}$$

We stress that we compute the analytic first derivatives of the regularizer but for the generalized Gauss-Newton scheme, we approximate the Hessians by

$$\begin{aligned} d^2 S_{s,1}^i(y) &= P_{(1,2,9)}^\top dA d^2 \phi_s dA P_{(1,2,9)}, \\ d^2 S_{v,1}^i(y) &= P_{(1,2,9,15)}^\top dV d^2 \phi_v dV P_{(1,2,9,15)}. \end{aligned}$$

The relatively fine partitioning of the voxels into 24 tetrahedra is computationally costly and a naive implementation may result in relatively high demands in terms of memory, even when using a sparse matrix format. This makes a matrix-based implementation prohibitive for practically relevant problem sizes although the matrices provide insight into the structure of the operators. Our implementation therefore provides a matrix-based version used for analysis, but also a matrix-free version that enables parallel processing of the voxels. This matrix-free implementation is fairly efficient in terms of memory requirements and runtime. In terms of memory requirements, the linear elastic and hyperelastic schemes are equivalent. In our numerical experiments we use this efficient implementation. Note that our discretization couples all nodal vertices via the face averages and the voxel center. Hence, the Hessian is relatively full and its inverse has smoothing properties; see Fig. 4.2 for a typical non-zero pattern of the Hessian.

The linear systems in the Gauss-Newton steps are solved using a preconditioned conjugate gradient scheme [31] with diagonal preconditioning, which takes advantage of our matrix-free implementation. Using this matrix-free representation and thus avoiding setup times for the matrix-representations gives further speedups as we expect and observe a small number of Gauss-Newton iterations on the finest discretization level.

**5. Results.** We present results for two applications that demonstrate the potential of the proposed hyperelastic regularization scheme. Our first example is academic and highlights the two main outstanding features of hyperelastic registration: its capability of handling large deformations and the guarantee for diffeomorphic transformations. For the ease of visualization, we use a 2D setting. The second, clinically

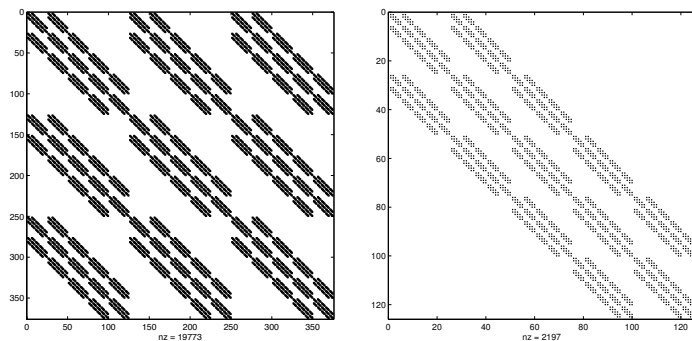


FIG. 4.2. Nonzero pattern of the Hessian (left) and the first  $125 \times 125$  block (right) with  $m = 4$ ; the grid has 64 nodes and the Hessian has 19,773 nonzeros.

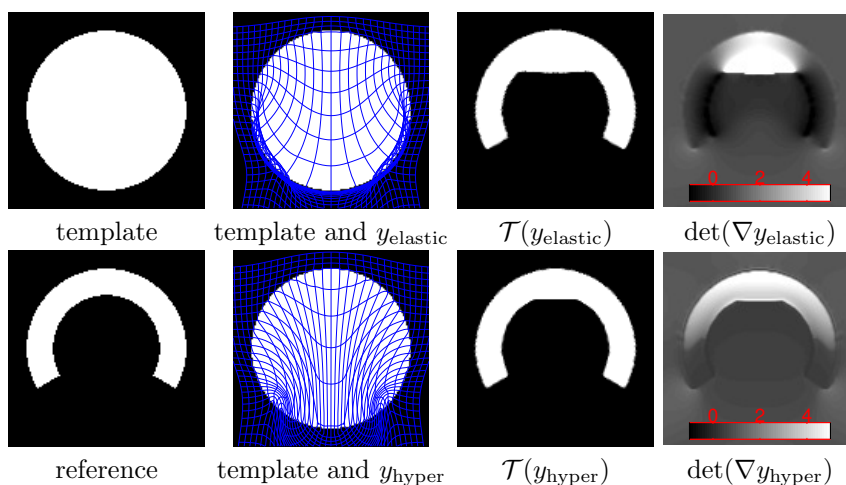


FIG. 5.1. Comparison of linear and hyperelastic registrations for 2D academic  $128 \times 128$  images as in [6]. Parameters used:  $\alpha = 1.000$ ,  $\mu = 1$ , and  $\lambda = 0$  (elastic),  $\alpha_1 = 100$ ,  $\alpha_2 = 0$ , and  $\alpha_3 = 20$  (hyperelastic);  $\det \nabla y_{\text{elastic}}(x) \in [-1.2, 19.4]$ ,  $\det \nabla y_{\text{hyper}}(x) \in [0.4, 5.5]$ .

relevant problem is related to a 3D registration problem from cardiac *Positron Emission Tomography* (PET); image courtesy by Fabian Gigengack from the European Institute for Molecular Imaging, Münster, Germany [18].

The first experiment is a direct comparison of a linear elastic scheme [37] and the novel hyperelastic registration. Motivated by [6], we aim to register a disc to a C shaped form such that large variations in the deformation field are to be expected. A  $128 \times 128$  resolution of the images and the  $L_2$ -norm based distance measure  $\mathcal{D}^{\text{SSD}}$  have been used. Figure 5.1 shows the template and reference image, a visualization of the transformation added to the template image, the deformed template images and a map of  $\det \nabla y$  for the linear elastic and hyperelastic registration, respectively.

The linear elastic approach (using the regularization  $\alpha = 1.000$ , and the Navier-Lamé constants  $\mu = 1$  and  $\lambda = 0$ ) has been driven beyond its limits:  $\det \nabla y(x) \in [-1.2, 19.4]$  and thus  $y$  is not diffeomorphic. For smaller values of  $\alpha$ , the scheme generates heavily distorted transformations and for larger values of  $\alpha$  the scheme yields unsatisfying transformed templates; see also [6, 36].

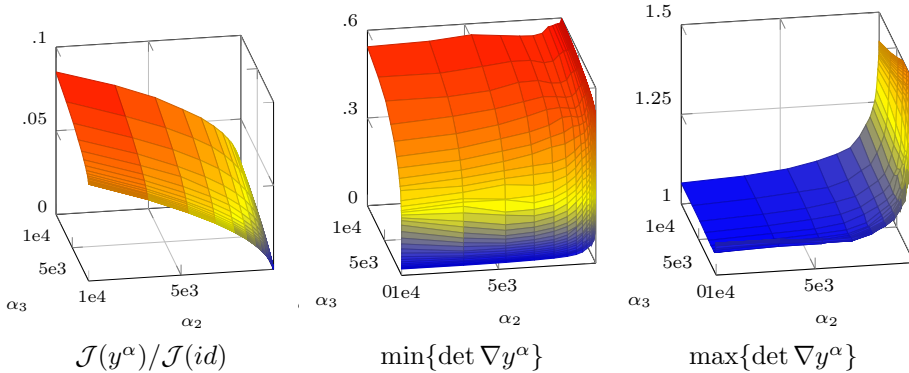


FIG. 5.2. Parameter dependence of the hyperelastic regularizer for the 3D cardiac PET registration problem. For  $\alpha_1 = 10$  fixed we vary the parameters  $\alpha_2, \alpha_3$  for surface and volume regularization logarithmically between  $10^{-3}$  and  $10^4$ . For the solutions  $y^\alpha$  we show the reduction of the objective function (left) and the minimal (center) and maximal (right) volumetric change.

The novel hyperelastic registration (with hand tuned parameter  $\alpha_1 = 100$ ,  $\alpha_2 = 0$ , and  $\alpha_3 = 20$ ) generates a diffeomorphic transformation with  $\det \nabla y(x) \in [0.4, 5.5]$ , which also yields a reasonably transformed template. Controlling the volumes of four triangles per pixel for the 2D case, we introduced an additional computational load and the runtime is approximately six times the time of our implementation of the elastic registration [37].

Our second application is related to the reconstruction of 3D PET images of a human heart. As the emphasis of this paper is on the numerical implementation of mass-preserving hyperelastic registration, we outline the underlying gating procedure only briefly. For a detailed discussion of this application as well as a clinical validation we refer to [18].

In PET reconstruction, a relatively long acquisition time of up to twenty minutes results in severe degradation of image quality due to respiratory and cardiac motion. So-called gating techniques are used to compensate for these motion artifacts [5]. In short, measurements are grouped into a number of gates, which relate to particular phases in the respiratory and cardiac cycle. For each gate, a reconstruction is computed which shows less motion blur but is also based on fewer counts and consequently of degraded quality. To take full advantage of all measurements the reconstructions are to be fused and image registration becomes inevitable to align the reconstructions of the different gates. For this application, it is important to acknowledge the fact that image intensities represent densities. Thus, the total number of events per tissue unit is a constant and a mass-preserving distance measure (2.3) is appropriate; see [44] for details. As outlined in Section 2, the registration functional thus requires higher order regularization. Since diffeomorphic but also large deformations are to be expected for the cardiac phases, hyperelastic registration is a method of choice.

In this experiment, we focus on a computationally most challenging registration subproblem, namely the registration of the extreme cardiac phases. The images are provided with an isotropic spatial resolution of 3.375 mm resulting in  $76 \times 76 \times 44$  voxels.

We investigate the dependence of the registration results on the regularization parameters  $\alpha_1, \alpha_2$  and  $\alpha_3$  as well as  $\phi_w$  and  $\phi_c$ ; see (2.6) and (2.7). To this end, we set  $\alpha_1$  to 50 and vary the parameters for surface and volume 31 equally spaced on a

logarithmical scale between  $10^{-1}$  and  $10^4$ . The double well function  $\phi_w$  is used for penalizing changes of surface area. The 961 registration problems are solved using two levels of a quarter and a half of the data resolution. Figure 5.2 visualizes the value of the objective function  $\mathcal{J}(y^\alpha)$  as a function of the regularization parameters  $\alpha$ , where  $y^\alpha$  denotes our numerical solutions. The figure also shows the minimal and maximal volumetric change. As expected, we observe a larger reduction of the objective function for smaller weights on the regularization functionals but still all transformations  $y^\alpha$  are diffeomorphic:  $\det(\nabla y^\alpha) \in [0.02, 1.73]$  for all experiments. This motivates the choice  $\alpha_2 = \alpha_3 = 10^{-1}$ . However, already a moderate regularization of surface and volume changes reduces the range of the determinant considerably, which leads us to pick slightly larger parameters. In our experiments, we used  $\alpha_2 = \alpha_3 = 10$ . Note that the landscapes are very smooth.

Figure 5.3 visualizes the final registration results for cardiac gated images of a systolic (reference) and a diastolic gate (template). The figure shows renderings of the heart wall in the reference, template, and transformed template images as well as a minimal intensity projections of the determinant  $\det \nabla y$ . For our mass-preserving hyperelastic registration we used the parameters  $\alpha_1 = 50, \alpha_2 = 10$  and  $\alpha_3 = 10$  and the double well surface function  $\phi_w$ . In this example, we use three levels in our multi-level strategy where the finest discretization equals the size of the original data. On the respective levels, 5, 3, and 2 iterations were performed and the total runtime was about 35 seconds on a Linux PC with a four core Intel Xeon X5670 @3,40 GHz using Matlab 2011a. Our scheme provides a diffeomorphic solution with  $\det \nabla y(x) \in [0.3, 2.1]$  and produces a transformed template that is visually identical to the reference.

Our last experiment compares the surface potentials  $\phi_w$  and  $\phi_c$ , see (2.7). Note that we proved existence of minimizing elements only for the convex surface penalty  $\phi_c$ . Our experiment shows that both surface potentials lead to very similar results in terms of distance and transformation. The distance reduction is 0.023% for  $\phi_c$  versus 0.029% for  $\phi_w$ . The mean and maximum Euclidean distance between the transformations are 0.38 mm and 2.68 mm in a representative rectangular region of interest around the heart. However, the differences of the models are observable in the volumetric changes. As to be expected, using the double-well penalty  $\phi_w$  yields a smaller range of  $[0.3, 2.1]$  versus  $[0.3, 2.4]$  for  $\phi_c$ . Therefore, we prefer the double well based model.

**6. Summary.** A novel hyperelastic registration technique has been proposed. The motivation is to provide a method that can deal with large transformation but at the same time provides sufficiently smooth and in particular diffeomorphic transformations. The new scheme is especially attractive for problems, where the distance measure can be phrased as a polyconvex function with respect to the transformation  $y$  and the Jacobian  $\nabla y$ . Examples of distance measures that involve  $\nabla y$  are related to densities and count processes and play an important role in Diffusion Tensor Imaging [40], Positron Emission Imaging [45, 18] and Single Photon Emission Computer Tomography [45].

A key feature of our hyperelastic models is that they result into infinite energy for non-diffeomorphic transformations. While this is a desirable property from an application point of view, it leads to a mathematically more challenging non-convex energy. We address this issue by using a polyconvex setting and by explicit control of length, surface, and volume. Using Ball's theorem, we proved existence of a minimizing element for the hyperelastic based registration energy  $\mathcal{J}$  with the convex surface

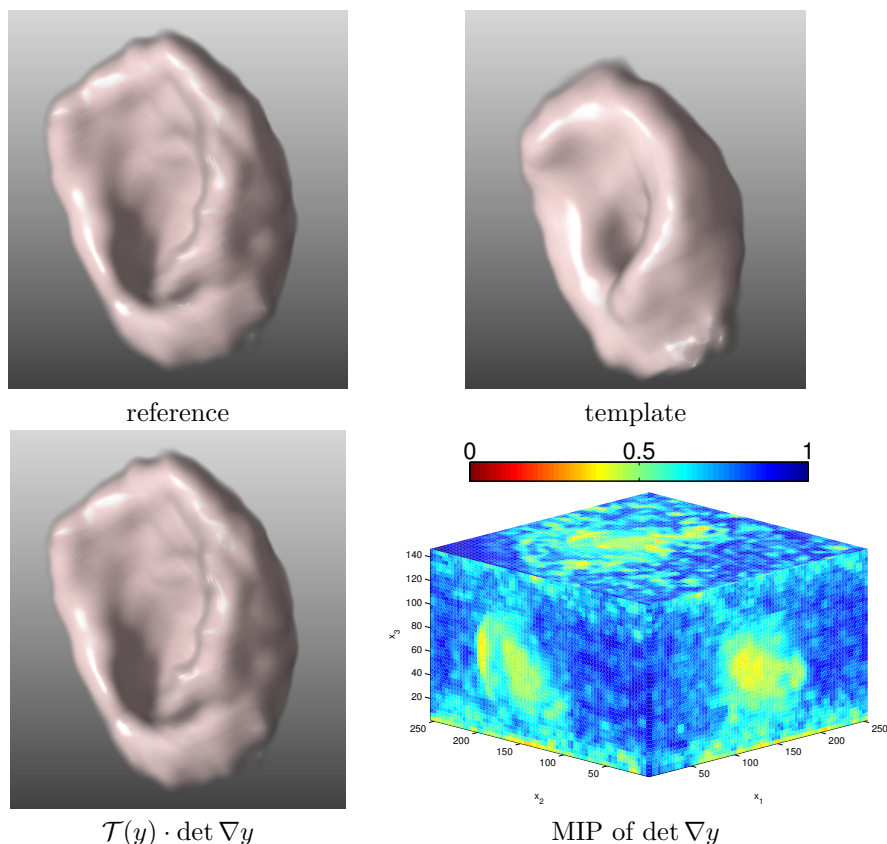


FIG. 5.3. Results for mass-preserving hyperelastic registration of 3D cardiac PET: reference (top left), template (top right), transformed and modulated template  $\mathcal{T}(y) \cdot \det \nabla y$  (bottom left), and minimum intensity projection (MIP) of the determinant of the Jacobian (bottom right); note that we show the minimal value of the determinant; since  $\det \nabla y(x) \in [0.3, 2.1]$ , the transformation is guaranteed to be diffeomorphic.

penalty  $\phi_c$ . This regularization is thus sufficient, but we do not know to what extent it can be weakened. In particular, we do not have proof for the proposed double-well surface penalty  $\phi_w$ , which is more appropriate from a modelling perspective and yields superior results in our examples.

However, the emphasis of this paper is on a numerical implementation of the hyperelastic registration scheme, where a proper measurement of the regularization energy is crucial. Acknowledging the given data structure, we use a nodal discretization with a tetrahedral partitioning of each voxel. The three invariants length, area, and volume are then measured using geometric primitives on each tetrahedron. We showed that such a discretization is sufficient to measure the regularization energy in the discrete setting. Moreover, we use a new partitioning as suggested by Heldmann [29]. This partition is based on 24 tetrahedra and avoids a bias with respect to a discretization direction as it has been observed for simpler (5 or 6 tetrahedra based) partitions and results in a smoother representation of the discrete transformation.

Our hyperelastic registration produces plausible and visually pleasing registration results. Most importantly, the transformation is guaranteed to be diffeomorphic and sufficiently smooth. This is supported not only by our theory but also controlled by

a precise numerical measurement. The downside is a non-neglectable computational load, even when using sparse matrix computations. Note that the hyperelastic scheme has the same complexity as the linear elastic scheme. The hyperelastic scheme requires more computations per voxel. Therefore, we also implemented a parallelized and matrix-free scheme. For this matrix-free code, memory consumption is kept at roughly the same level as for the linear elastic schemes and reasonable runtimes are obtained. Future work will address further improvements of the algorithm and its implementation.

Finally we presented two applications, demonstrating the potential of the hyperelastic registration. The first one is an example from Christensen [6], which has been designed to uncover the limitations of a linear elastic model for image registration. As to be expected, the hyperelastic scheme gives a reasonable result while a linear elastic scheme does not. The second example is a 3D mass-preserving PET registration. As our distance measure depends nonlinearly on  $\nabla y$ , higher order regularization becomes mandatory. To our best knowledge, hyperelastic registration is presently the only approach for this type of problems. As it turns out, our scheme yields amazingly good results. Related work addresses the clinical evaluation of the relevance of our mass-preserving hyperelastic registration results [18].

We used the FAIR software as a computational framework. Moreover, the implementation of our new hyperelastic regularizer has been integrated to FAIR's new version which is available from SIAM website <http://www.siam.org/books/fa06/>.

**7. Acknowledgments.** We thank the two anonymous reviewers for their extremely valuable comments and corrections of our manuscript. We are indebted to Stefan Heldmann for various discussions and for pointing out the partition used in our discretization. We are also indebted to Fabian Gigengack for providing such a challenging registration problem and the *Deutsche Forschungsgemeinschaft's* (DFG) Collaborative Research Center SFB 656 for the underlying data. Jan Modersitzki also acknowledges the support of the European Union and the State of Schleswig-Holstein (MOIN CC: grant no. 122-09-053). Martin Burger acknowledges financial support by the DFG via SFB 656 and BU 2327/2-1.

#### REFERENCES

- [1] R. BAJCSY AND S. KOVAČIĆ, *Toward an individualized brain atlas elastic matching*, Tech. Report MS-CIS-86-71 Grasp Lap 76, Dept. of Computer and Information Science, Moore School, University of Philadelphia, 1986.
- [2] J. M. BALL, *Convexity conditions and existence theorems in nonlinear elasticity*, Archive for rational mechanics and Analysis, 63 (1976), pp. 337–403.
- [3] B. BEUTHIEN, *Private communication*, 2010. Institute of Mathematics and Image Computing, Lübeck.
- [4] C. BROIT, *Optimal Registration of Deformed Images*, PhD thesis, Computer and Information Science, University of Pennsylvania, USA, 1981.
- [5] F. BÜTHER, M. DAWOOD, L. STEGGER, F. WÜBBELING, M. SCHÄFERS, O. SCHÖBER, AND K.P. SCHÄFERS, *List mode-driven cardiac and respiratory gating in PET*, Journal of Nuclear Medicine, 50 (2009), pp. 674–681.
- [6] G.E. CHRISTENSEN, *Deformable Shape Models for Anatomy*, PhD thesis, Sever Institute of Technology, Washington University, USA, 1994.
- [7] P. G. CIARLET, *Mathematical Elasticity: Three-dimensional Elasticity*, North Holland, 1988.
- [8] A. COLLIGNON, A. VANDERMEULEN, P. SUETENS, AND G. MARCHAL, *3D multi-modality medical image registration based on information theory*, Kluwer Academic Publishers: Computational Imaging and Vision, 3 (1995), pp. 263–274.
- [9] B. DACOROGNA, *Direct methods in the calculus of variations*, Springer Verlag, 2008.

- [10] M. DROSKE, *On variational problems and gradient flows in image processing*, PhD thesis, Gerhard-Mercator-Universität Duisburg, (2005).
- [11] M. DROSKE AND M. RUMPF, *A variational approach to non-rigid morphological registration*, SIAM Appl. Math., 64 (2004), pp. 668–687.
- [12] M. DROSKE, M. RUMPF, AND C. SCHALLER, *Non-rigid morphological registration and its practical issues*, in Proc. ICIP '03, IEEE International Conference on Image Processing, Sep. 2003, Barcelona, Spain, 2003.
- [13] L. C. EVANS, *Partial Differential Equations*, Vol. 19 of Graduate Studies in Mathematics, American Mathematical Society, Providence, USA, 1999.
- [14] B. FISCHER AND J. MODERSITZKI, *Combination of automatic non-rigid and landmark based registration: the best of both worlds*, In: M. Sonka and J. M. Fitzpatrick (eds.), Medical Imaging 2003: Image Processing, Proceedings of the SPIE 5032 (2003), pp. 1037–1048.
- [15] ———, *Combining landmark and intensity driven registrations*, PAMM, 3 (2003), pp. 32–35.
- [16] ———, *Ill-posed medicine – an introduction to image registration*, Inverse Problems, 24 (2008), pp. 1–19.
- [17] J. M. FITZPATRICK, D. L. G. HILL, AND C. R. JR. MAURER, *Image registration*, In: M Sonka and JM Fitzpatrick (eds.), Handbook of Medical Imaging, Volume 2: Medical Image Processing and Analysis, SPIE (2000), pp. 447–513.
- [18] F. GIGENGACK, L. RUTHOTTO, M. BURGER, C. H. WOLTERS, X. JIANG, AND K. P. SCHÄFFERS, *Motion correction in dual gated cardiac PET using mass-preserving image registration*, IEEE Transactions on Medical Imaging, 31(3), pp. 698–712 (2012).
- [19] C. GLASBEY, *A review of image warping methods*, Journal of Applied Statistics, 25 (1998), pp. 155–171.
- [20] A. ARDESHIR GOSHTASBY, *2-D and 3-D Image Registration*, Wiley Press, New York, 2005.
- [21] E. HABER, S. HELDMANN, AND J. MODERSITZKI, *A scale-space approach to landmark constrained image registration*, in Proceedings of the Second International Conference on Scale Space Methods and Variational Methods in Computer Vision (SSVM), Springer LNCS, 2009, pp. 1–12.
- [22] E. HABER, R. HORESH, AND J. MODERSITZKI, *Numerical methods for constrained image registration*, Numerical Linear Algebra with Applications, 17 (2010), pp. 343–359.
- [23] E. HABER AND J. MODERSITZKI, *Numerical methods for volume preserving image registration*, Inverse Problems, Institute of Physics Publishing, 20 (2004), pp. 1621–1638.
- [24] ———, *Image registration with a guaranteed displacement regularity*, IJCV, 1 (2006). DOI: 10.1007/s11263-006-8984-4.
- [25] ———, *Intensity gradient based registration and fusion of multi-modal images*, in Medical Image Computing and Computer-Assisted Intervention – MICCAI 2006, C Barillot, DR Haynor, and P Hellier, eds., vol. 3216, Springer LNCS, 2006, pp. 591–598.
- [26] C. LE GUYADER AND L. A. VESE, *A combined segmentation and registration framework with a nonlinear elasticity smoother*, Computer Vision and Image Understanding, 115(12), pp. 1689–1709 (2011).
- [27] J. HADAMARD, *Sur les problèmes aux dérivées partielles et leur signification physique*, Princeton University Bulletin, (1902), pp. 49–52.
- [28] J HAJNAL, D HAWKES, AND D HILL, *Medical Image Registration*, CRC Press, 2001.
- [29] S. HELDMANN, *Private communication*, 2011. Fraunhofer MEVIS, Project group Image Registration, Lübeck.
- [30] S. HENN, *A multigrid method for a fourth-order diffusion equation with application to image processing*, SIAM J. Sci. Comput., 27 (2006), pp. 831–849.
- [31] M. R. HESTENES AND E. STIEFEL, *Methods of conjugate gradients for solving linear systems*, J. Res. Nat. Bur. Stand., 49 (1952), pp. 409–436.
- [32] W. HINTERBERGER, O. SCHERZER, C. SCHNÖRR, AND J. WEICKERT, *Analysis of optical flow models in the framework of calculus of variations*, Num. Funct. Anal. Opt., 23 (2002), pp. 69–89.
- [33] C.O. HORGAN, *Korn's inequalities and their applications in continuum mechanics*, SIAM review, 37 (1995), pp. 491–511.
- [34] W. A. LIGHT, *Variational methods for interpolation, particularly by radial basis functions*, in Numerical Analysis 1995, DF Griffiths and GA Watson, eds., London, 1996, Longmans, pp. 94–106.
- [35] J. B. ANTOINE MAINTZ AND M. A. VIERGEVER, *A survey of medical image registration*, Medical Image Analysis, 2 (1998), pp. 1–36.
- [36] J. MODERSITZKI, *Numerical Methods for Image Registration*, Oxford University Press, New York, 2004.
- [37] ———, *FAIR: Flexible Algorithms for Image Registration*, SIAM, Philadelphia, 2009.

- [38] J. NOCEDAL AND S. J. WRIGHT, *Numerical optimization*, Springer, New York, 1999.
- [39] J. OLESCH, N. PAPANBERG, T. LANGE, M. CONRAD, AND B. FISCHER, *Matching CT and ultrasound data of the liver by landmark constrained image registration*, vol. 7261, SPIE (2009).
- [40] J. OLESCH, L. RUTHOTTO, H. KUGEL, S. SKARE, B. FISCHER, AND C. H. WOLTERS, *A variational approach for the correction of field-inhomogeneities in EPI sequences*, in Proc. SPIE 7623 (2010).
- [41] W. PECKAR, C. SCHNÖRR, K. ROHR, AND H. S. STIEHL, *Parameter-free elastic deformation approach for 2D and 3D registration using prescribed displacements*, J. Math. Imaging and Vision, 10 (1999), pp. 143–162.
- [42] J.P.W. PLUIM, J.B.A. MAINTZ, AND M.A. VIERGEVER, *Mutual-information-based registration of medical images: a survey*, IEEE TMI, 22 (1999), pp. 986–1004.
- [43] C. PÖSCHL, J. MODERSITZKI, AND O. SCHERZER, *A variational setting for volume constrained image registration*, Inverse Problems and Imaging, 4 (2010), pp. 500–522.
- [44] L. RUTHOTTO, *Mass-preserving registration of medical images*, Diploma thesis (written in english), University of Münster, 2010.
- [45] K. THIELEMANS, E. ASMA, AND R.M. MANJESHWAR, *Mass-preserving image registration using free-form deformation fields*, in Nuclear Science Symposium Conference Record (NSS/MIC), IEEE, (2009), pp. 2490–2495.
- [46] J.-P. THIRION, *Image matching as a diffusion process: an analogy with Maxwell’s demons*, Medical Image Analysis, 2 (1998), pp. 243–260.
- [47] P. VIOLA AND W. M. WELLS III, *Alignment by maximization of mutual information*, (1995), pp. 16–23. IEEE 1995.
- [48] J. WEICKERT AND C. SCHNÖRR, *A theoretical framework for convex regularizers in PDE-based computation of image motion*, IJCV, 45 (2001), pp. 245–264.
- [49] I. YANOVSKY, C. LE GUYADER, A. LEOW, P. THOMPSON, AND L. VESE, *Unbiased volumetric registration via nonlinear elastic regularization*, Mathematical Foundations of Computational Anatomy, (2008), pp. 1–8.
- [50] B. ZITOVÁ AND J. FLUSSER, *Image registration methods: a survey*, Image and Vision Computing, 21 (2003), pp. 977–1000.